地震研究所彙報
Bull. Earthq. Res. Inst.
Univ. Tokyo
Vol. 81 (2006) pp. 247–251

Resolving the Source Parameters of the Parkfield Earthquake by Multiple Inversions of Different Data Sets

Ralph J. Archuleta[1)]*, Susana Custódio[1)] and Pencheng Liu[2)]

[1)] Dept. of Earth Science and Institute for Crustal Studies, University of California, Santa Barbara, CA 93106
[2)] Institute for Crustal Studies, University of California, Santa Barbara, CA 93106

Abstract

Inverting data to infer the kinematic source parameters of faulting has many inherent difficulties including incomplete knowledge of the structure of the medium, insufficient data in both quantity and quality and nonlinear relationships between the data and the parameters of the model. Consequently most models of faulting are poorly resolved. Because the Parkfield segment of the San Andreas Fault was the location of an on-going earthquake prediction experiment, the 40 km segment was closely monitored when a M_W 6.0 earthquake occurred on 28 September 2004. By subdividing the 43 near-source strong motion accelerometers into 12 overlapping subsets of 20 stations or more, we invert for the kinematic parameters of the faulting. This procedure allows us to determine the mean and variance of the kinematic parameters as if the same earthquake were recorded by 12 different distributions of stations. The mean value of each parameter is compared to the parameter found by inverting all 43 stations. Because the relationship between some of the parameters and the data is nonlinear, we also invert all the data using different initial conditions. This leads to a distribution of parameters with a mean and a standard deviation that provide insight into how well the parameters are resolved on the fault.

Key words : Inversion, strong-motion, Parkfield, slip, earthquake

1. Introduction

The 28 September 2004, the M_w 6.0 Parkfield earthquake is one of the most densely recorded earthquakes for near-source ground-motion. To infer the kinematic parameters that describe the faulting we invert the data from 43 near-source strong-motion accelerometers (Shakal *et al.,* 2004) (Figure 1). We use a non-linear global inversion yields slip amplitude, slip rake, rupture velocity, and rise time on the fault (Liu and Archuleta, 2004). By using subsets of the data, we study the dependence of the kinematic solutions on data input. To determine how robust the model we have used various techniques. 1) The 43 accelerometers were subdivided into 12 groups of approximately 20–25 stations. Each group had approximately the same azimuthal and distance distribution with respect to the fault. The resulting 12 rupture models allow us to determine a mean and a standard deviation for the kinematic parameters. 2) Data from a given subset of stations were inverted to find a model. This rupture model was used to predict ground motion at the stations not used in the inversion.

2. Data and Inversion Method

The 43 acceleration records were integrated into velocity waveforms, and then filtered in a pass-band of 0.16 *Hz*–1.0 *Hz*. The lower limit is dictated by digitization resolution. The upper frequency limit is determined by the resolution of the velocity structure.

The nonlinear global inversion method of Liu and Archuleta (2004) was used to find the kinematic parameters to describe the rupture model for the Parkfield earthquake. This inversion procedure relies on a simulated annealing algorithm to efficiently find a model that best fits the observed data. The purpose of the inversion is to minimize a misfit function (Liu and Archuleta, 2004, equation 9b) that meas-

* e-mail: ralph@crustal.ucsb.edu

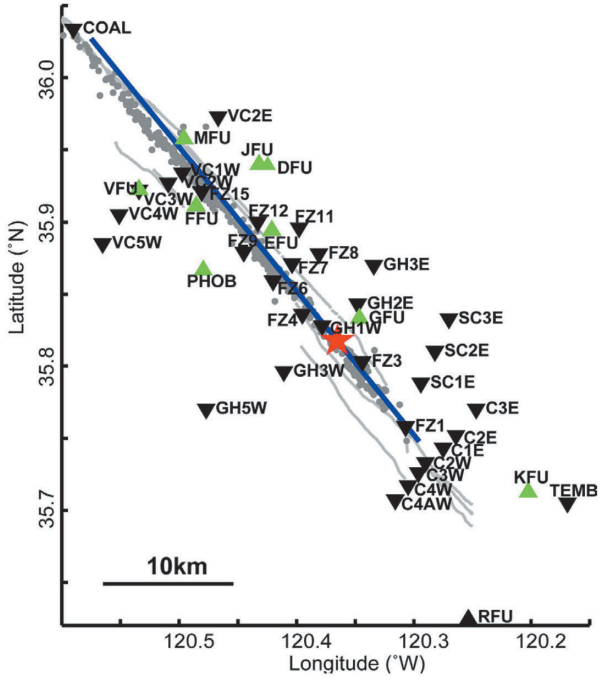

Fig. 1. Accelerometers (green, USGS; black, CGS) near the San Andreas Fault (light grey lines). Epicenter is the star. Blue line is our approximation to the fault. Grey circles are aftershock epicenters (Hardebeck and Michael, 2004).

ures the difference between synthetic and observed velocity waveforms. In addition, the misfit function imposes smoothness and seismic moment constraints on the model being derived. Because the event is primarily strike slip we downweight the vertical component by a factor of 10 relative to the two horizontal components.

In our model the hypocenter is at 35.817° N, 120.365° W and 8.1km depth—this is deeper than the USGS location but provides a closer fit to the S wave arrival for the accelerometers near the epicenter with our assumed velocity structure. We assume fault geometry: strike, 141°; dip 89°; length, 40 km and depth, 15 km. Because there was no co-seismic surface slip (Langbein *et al.*, 2004), we allow no slip for depths less than 0.5 km.

Using the frequency-wavenumber method of Zhu and Rivera (2003), we compute Green's functions on a 500 m × 500 m grid. We use a bilateral 1D velocity model adapted from the 3D velocity models of Eberhart-Phillips and Michael (1993) and Thurber *et al.* (2003). The 1D velocity model (Table 1) takes into account the velocity contrast between the granitic Salinian block southwest of the fault (faster) and the

Table 1: Velocity and Attenuation Structure

Thick (km)	Dens (kg/m^3)	Vp (km/s)	Vs (km/s)	Qp	Qs
Structure Southwest of the San Andreas Fault					
1.0	2000	2.0	1.1	70	35
1.0	2300	3.5	2.0	140	80
1.0	2300	4.5	2.5	300	200
0.5	2500	5.2	3.0	390	230
2.3	2700	5.7	3.2	500	260
8.3	2700	6.2	3.6	500	300
3.0	2800	6.8	3.6	510	300
3.3	2800	6.8	4.3	510	550
∞	2800	7.3	4.3	800	550
Structure Northeast of the San Andreas Fault					
1.0	2000	2.0	1.1	70	35
0.8	2300	3.5	2.2	140	80
0.3	2300	4.2	2.8	300	200
1.3	2300	4.8	2.7	320	200
0.5	2300	5.2	2.8	380	200
4.4	2700	5.3	3.2	380	250
4.4	2800	5.7	3.7	500	290
4.8	2800	6.5	3.8	500	290
2.8	2800	6.7	4.3	510	530
∞	2800	7.3	4.3	800	550

Franciscan terrain northeast of the fault (slower).

Source parameters are inverted on a 2 km × 2 km grid. Slip *s(t)* at each node is described by time function given in Equation 1. The rise time (T) is split into an accelerating (T1) and a decelerating (T2) rise times, such that T = T1 + T2. Both T1 and T2 are independent parameters in the inversion.

$$\frac{ds}{dt} = \begin{cases} A\left[\sin\left(\frac{t}{T_1}\frac{\pi}{2}\right)\right], \; if \; 0 < T < T_1 \\ A\left[1+\cos\left(\frac{t-T_1+T_2}{T_2}\frac{\pi}{2}\right)\right], \; if \; T_1 < T < T_1 \end{cases} \quad (1)$$

As mentioned earlier the 43 stations are subdivided into groups that have approximately the same distance and azimuthal distribution with respect to the fault. For example, in Figure 2 we show two such groups.

3. Results

We inverted the data for 12 different subsets of the stations. The basic results are summarized in a single plot (Figure 3) where we show the mean, variance and coefficient of variation (std/mean) of the kinematic parameters based on 12 inversions as well as the result of inverting all the stations. First note

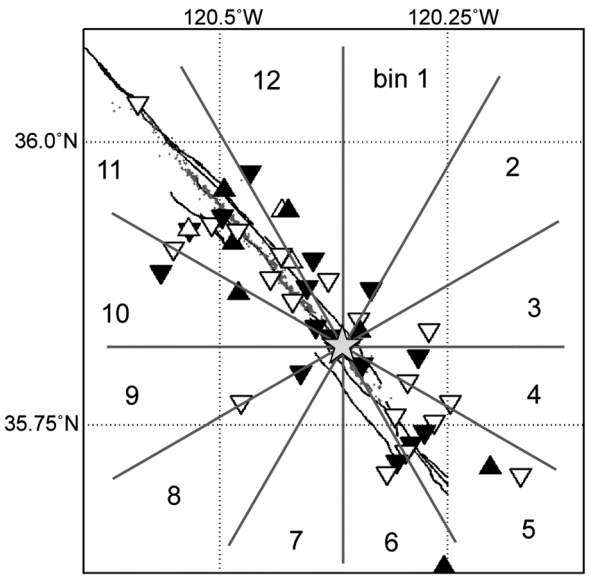

Fig. 2. Group A-22 stations (black). Group B-21 stations (white). Inverted triangles-CGS stations; triangles-USGS stations; small gray dots-aftershocks (Hardebeck and Michael, 2004); star-epicenter.

that the slip distribution found from inverting all of the stations is quite similar to that found for the average of the 12 inversions. The largest slip ~70 cm occurs near the hypocenter but slightly to the southeast. Most of the large-amplitude slip occurs at depths less than 10 km. There is one small deep patch (about 10 km NW of the hypocenter) that is evident on the average of the 12 inversions (Row B) as well as the inversion of all the data (Row A). This suggests that this patch of slip is an element of the earthquake. Otherwise, the slip is basically negligible below 10 km. The slip that occurs between 5 and 10 km depth about 10–20 km NW of the hypocenter is not well resolved. The inversions require slip in this region, but one can see that the standard deviation (Row C) is large in this area of the fault. The rake is almost exclusively right-lateral. The rise time is small, generally less than 1.0 s. The local rupture velocity is more difficult to quantify. The inversion solves for an average rupture velocity between the hypocenter and any point of the fault (Liu and Archuleta, 2004), but the local rupture velocity over

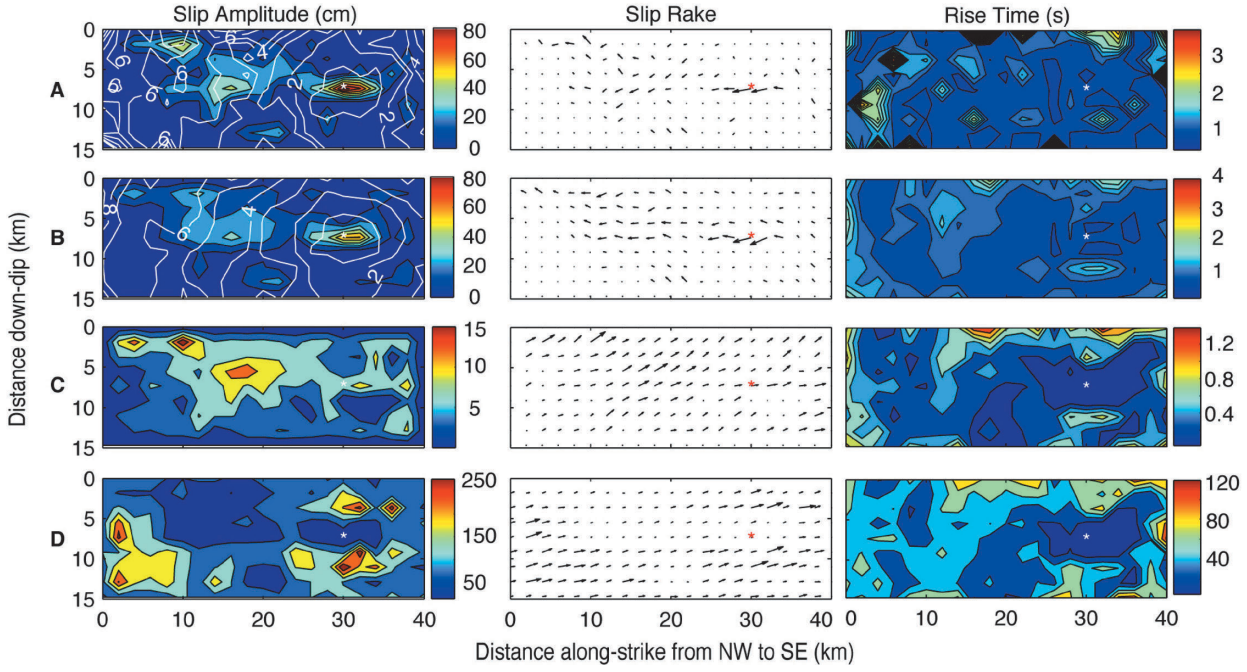

Fig. 3. The kinematic parameters are plotted on the assumed fault plane. The asterisk marks the hypocenter. First column are contours of slip amplitude (cm) with the rupture time shown as white lines at 1 sec intervals. Second column is slip vector showing the amplitude and rake; third column are contour plots of rise time (sec). In Row A we show the results of inverting all of the seismograms. In Row B we show the average of the 12 inversions. In Row C we contour the standard deviation for the 12 inversions. In Row D we contour the coefficient of variation (standard deviation/mean). The average retains the coherent features from the 12 different models. The coefficient of variance shows the percentage of variability of the models with respect to the average.

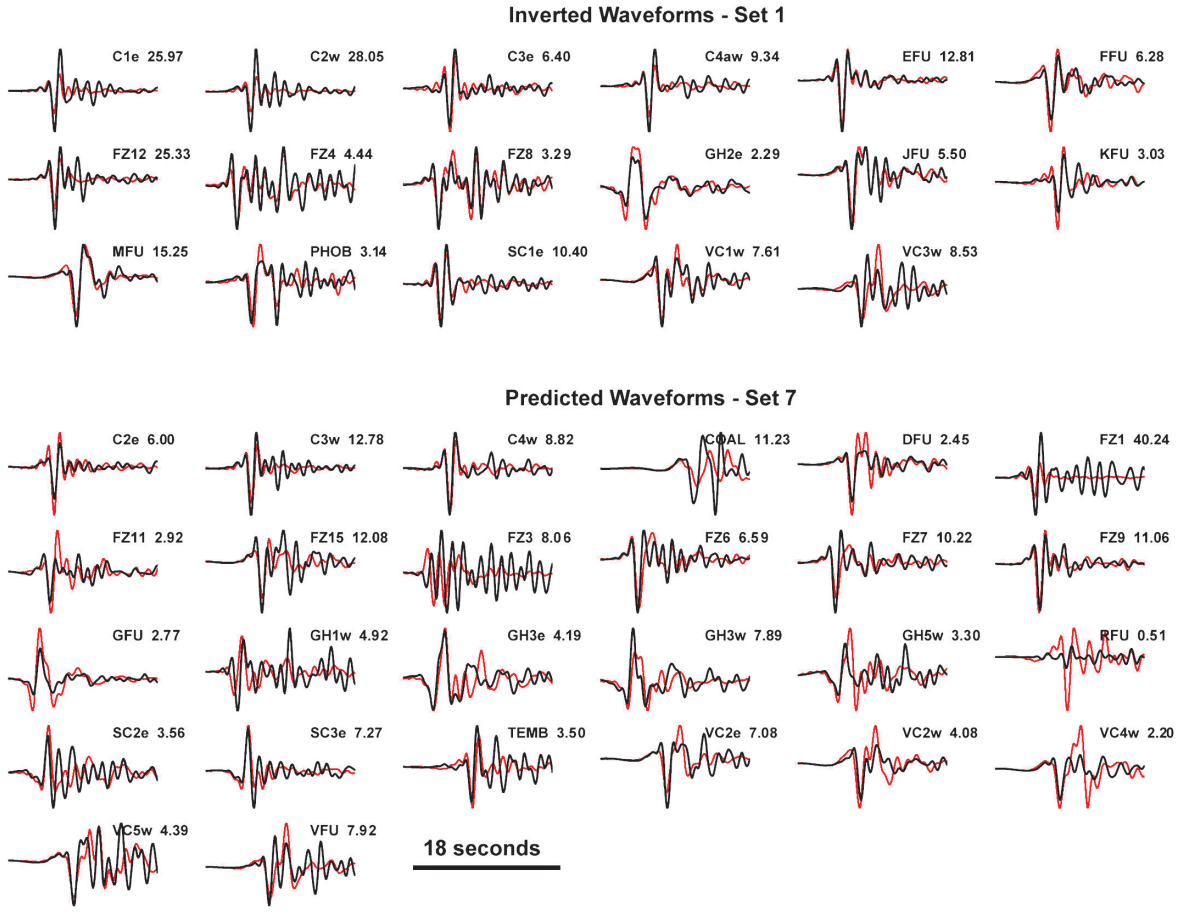

Fig. 4. Eighteen seconds of the velocity waveforms are shown for the transverse component of motion. The transverse component is the component perpendicular to a straight line between the epicenter and the station. Data are shown as black and synthetics are shown as red. Each trace is scaled to a fixed height; peak amplitudes are shown in cm/s. The 17 stations (Set 1) were used to derive a faulting model; the 26 stations of Set 7 are the complementary set of stations. The waveforms (Set 7) are predicted from the model determined by Set 1. There is fairly good agreement at most stations but late arrivals in Set 7 are not fit as well as those fit by inversion.

different parts of the fault can be of more interest. The white lines superposed on the slip amplitude (Rows A and B, Figure 3) are the locations of the rupture front at 1 sec intervals. The rupture velocity near the hypocenter is supershear out for about 2 seconds. As the rupture proceeds to the NW, the speed slows down about 15 km NW of the hypocenter, but suddenly speeds up again.

As an example of the fit to the data we show bandpassed particle velocity time series for synthetics and data (Figure 4). In general, we found is that the misfit function summed over the predicted stations is about twice what we find for the inverted stations. However, in looking at the inverted and predicted ground motions, a factor of two in misfit does not mean that there is a major discrepancy. It has more to do with misfits to the smaller amplitudes.

4. Summary

Because of the extensive near-source dataset we have investigated the dependence of faulting models on the stations used for inversion. We show that the average of 12 inversions is similar to that found by inverting all of the data. However, the standard deviation, that can only be determined from multiple inversions, demonstrates which parts of the fault are better resolved than others.

Acknowledgments

Data were obtained from the California Geological Survey and the United States Geological Survey.

Custódio has support from a fellowship from the Portuguese Foundation for Science and Technology. This research is supported by the National Science Foundation, EAR-0512000 and the Southern California Earthquake Center (SCEC) under an NSF Cooperative Agreement EAR-0106924 and USGS Cooperative Agreement 02HQAG0008. The SCEC contribution number for this paper is 1076. This is ICS contribution 0802.

References

Eberhart-Phillips, D and A. J. Michael (1993), Three-dimensional velocity structure, seismicity, and fault structure in the Parkfield region, central California, *J. of Geophys. Res., 98,* 15737–15758.

Hardebeck, J. L., and A. Michael (2004), Earthquake locations before and after the 2004 M6.0 Parkfield earthquake, *Eos Trans. AGU, 85,* Fall Meet. Suppl., Abstract S 51C–0170W.

Langbein, J., R. Borcherdt, D. Dreger, J. Fletcher, J. L. Hardebeck, M. Hellweg, C. Ji, M. Johnston, J. R. Murray, R. Nadeau, M. J. Rymer, and J. Treiman (2005), Preliminary report on the 28 September 2004, M6.0 Parkfield, California, earthquake, *Seism. Res. Letters, 76,* 10–26.

Liu, P., and R. J. Archuleta (2004), A new nonlinear finite fault inversion with three-dimensional Green' s functions: Application to the 1989 Loma Prieta, California, earthquake, *J. Geophys. Res., 109,* doi: 10.1029/2003JB 002625.

Shakal, A., V. Graizer, M. Huang, R. Borcherdt, H. Haddadi, K. Lin, C. Stephens, and P. Roffers (2005), Preliminary Analysis of Strong-motion Recordings from the 28 September 2004 Parkfield, California Earthquake, *Seism. Res. Letters, 76,* 27–39.

Thurber, C., S. Roecker, K. Roberts, M. Gold, L. Powell, and K. Rittger (2003), Earthquake locations and three-dimensional fault zone structure along the creeping section of the San Andreas Fault near Parkfield, CA: Preparing for SAFOD, *Geophys. Res. Let., 30,* doi: 10.1029/2002GL016004.

Zhu, L. and Rivera, L. A. (2002), A note on the dynamic and static displacements from a point source in multilayered media, *Geophys. J. Int., 148,* 619-627, doi: 10.1046/j. 1365–246X.2002.01610.

(Received December 23, 2005)
(Accepted August 14, 2006)